Nonlinear Wave Kinematics near the Ocean Surface

P. B. SMIT

NorthWest Research Associates, El Granada, California

T. T. JANSSEN

Spoondrift Technologies, Inc., Half Moon Bay, California

T. H. C. HERBERS

NorthWest Research Associates, El Granada, California

(Manuscript received 20 December 2016, in final form 19 March 2017)

ABSTRACT

Estimation of second-order, near-surface wave kinematics is important for interpretation of ocean surface remote sensing and surface-following instruments, determining loading on offshore structures, and understanding of upper-ocean transport processes. Unfortunately, conventional wave theories based on Stokes-type expansions do not consider fluid motions at levels above the unperturbed fluid level. The usual practice of extrapolating the fluid kinematics from the unperturbed free surface to higher points in the fluid is generally reasonable for narrowband waves, but for broadband ocean waves this results in dramatic (and nonphysical) overestimation of surface velocities. Consequently, practical approximations for random waves are at best empirical and are often only loosely constrained by physical principles. In the present work, the authors formulate the governing equations for water waves in an incompressible and inviscid fluid, using a boundary-fitted coordinate system (i.e., sigma or s coordinates) to derive expressions for near-surface kinematics in nonlinear random waves from first principles. Comparison to a numerical model valid for highly nonlinear waves shows that the new results 1) are consistent with second-order Stokes theory, 2) are similar to extrapolation methods in narrowband waves, and 3) greatly improve estimates of surface kinematics in random seas.

1. Introduction

Wave-induced near-surface kinematics of nonlinear random waves are important, for example, for understanding remote sensing signals (e.g., Rascle et al. 2014) and for interpreting motions of wave-following instruments (e.g., Herbers et al. 2012; Herbers and Janssen 2016), wave forcing on offshore structures (e.g., Donelan et al. 1992; Schløer et al. 2011; Deng et al. 2016), oil droplet transport (e.g., Geng et al. 2016), and wave-driven surface flows and Stokes drift in random waves (e.g., Stokes 1847; Monismith et al. 2007; Herbers and Janssen 2016).

Despite the importance of near-surface kinematics, Stokes-type wave theories consider the fluid domain to be vertically confined between the (impermeable) bottom $z = -h$ and the unperturbed free surface $z = 0$ and do not describe the fluid kinematics in the region above $z = 0$ (e.g., Longuet-Higgins and Stewart 1960; Hasselmann 1962; Sharma and Dean 1981). The omission of the near-surface kinematics in these theories is a consequence of the fact that nonlinear effects associated with free-surface deformations enter the solution through Taylor expansions of the free-surface boundary conditions around $z = 0$, but the fluid domain is not modified accordingly. In other words, the deformations of the free surface do not enter the domain for which the field equations are solved. As a result, the vertical structure of the velocity potential for a free (or bound) wave with wavenumber k in deep water takes the general form

$$\exp(kz) \quad -h < z < 0,$$

which leaves the region $0 < z < \eta$ undefined. Two common (and logical) extrapolation methods to estimate wave-induced kinematics near the surface are 1) extrapolate the solution to the free surface ($z = \eta$) using the analytic solution dictated by the Laplace equation (e.g., Baldock et al. 1996) or 2) use a Taylor series based around $z = 0$ to predict velocities above $z = 0$ (e.g., Rodenbusch

Corresponding author: P. B. Smit, pieterbartsmit@gmail.com

DOI: 10.1175/JPO-D-16-0281.1

and Forristall 1986) In deep water these two approaches give

$$\exp(kz) \quad \text{and} \quad 1 + kz \tag{1}$$

for $z > 0$, respectively, whereas for $z < 0$ we always have $\exp(kz)$. Both approaches—although distinct—appear reasonable within the context of weakly nonlinear narrowband waves. After all, in narrowband waves we can define a representative wave amplitude a and wavenumber k_0, where in this context a is a representative extrapolation scale whereas k_0^{-1} is a typical vertical scale of the motion, so that both methods are accurate to $O(\varepsilon^2)$ for $\varepsilon = k_0 a \ll 1$ and thus identical in the context of second-order theory. However, these approaches do differ in how they constrain the problem. Analytical extrapolation maintains continuity in the region $z > 0$ as it ensures that the solution obeys the Laplace equation. However, the solution is inconsistent with the Taylor-expanded free-surface boundary conditions, which leaves an unbalanced term of $O(\varepsilon^3)$. Linear extrapolation, on the other hand, is exactly consistent with the free-surface boundary condition to second order since it also represents the lowest-order term of a Taylor expansion. However, it is not consistent with continuity and leads to unbalanced terms of $O(\varepsilon^3)$ in the Laplace equation.

In irregular waves, we can still define a single, characteristic vertical scale for the surface elevation (for instance, the root-mean-square crest height η_{rms}), but the relevant vertical scale k^{-1} associated with the wave components varies with frequency. As a consequence, even if the mean steepness ε is moderate, the vertical scale of the wave motion in the tail of the spectrum is very short, such that $k\eta_{\text{rms}}$ can be $O(1)$ when these short waves ride on the crest of longer waves. In particular for analytical extrapolation, which is the conventional way to estimate the fluid velocities over the water column (and which we will alternatively refer to as conventional theory), this becomes problematic. When evaluated at a representative vertical elevation $z = \eta_{\text{rms}}$, we find that $\exp(k\eta_{\text{rms}})$ grows exponentially with increasing k, so that for typical roll-off in the spectral tail (e.g., $\propto k^{-5/2}$), the kinematic estimates near the surface grow without bounds. As a result, a perturbation approach breaks down, and extrapolation errors are large and result in unphysical results (e.g., Donelan et al. 1992).

To illustrate the issue in random waves, consider the extrapolated pressure field in multidirectional irregular waves (see Fig. 1). The analytical extrapolation leads to large nonzero pressures at the surface, which clearly violates the assumption of $p = 0$ at the free surface (see Fig. 1). In contrast, when using linear extrapolation, the surface pressure is accurately constrained to zero (it is consistent with applied boundary conditions), but it leads to an unrealistic (and nonphysical) vertical profile with a kink at $z = 0$ (see Fig. 1, right panel). Further, when $\eta < 0$, both extrapolation methods reduce to the analytical profile, and nonzero pressures at the surface occur in either approximation.

To bypass the shortcomings of extrapolation methods in random waves, empirical approaches to estimate near-surface wave kinematics have been proposed. These approaches either simply remove high-frequency components or use an empirical vertical structure function [predominantly in offshore engineering literature (e.g., Wheeler 1970; Lo and Dean 1986; Donelan et al. 1992)] Perhaps the most widely used method is that by Wheeler (1970), who proposed to stretch the profile valid for the undisturbed domain to fit the instantaneous domain. Although these approaches alleviate some of the symptoms of the fundamental shortcomings of a Stokes-type expansion in a fluid domain bounded by the undisturbed free surface $z = 0$, they do not fundamentally resolve them. Furthermore, they are based on heuristic arguments, not constrained by first principles, and can lead to unexpected results.

In this work we propose a different approach, which is a natural and first-principle extension of Stokes-type theories, and unambiguously defines the near-surface wave kinematics up to the second-order for multidirectional, irregular waves. To do this we transform the vertical domain to a boundary-fitted coordinate system (e.g., as in Blumberg and Mellor 1987; Shchepetkin and McWilliams 2005; Engsig-Karup et al. 2009; Chalikov et al. 2014) and determine approximate series solutions to the transformed system of equations. The resulting equations describe a complete second-order wave theory for irregular waves, which is consistent with Stokes theory, includes the correct near-surface kinematics, remains valid if the extrapolation scale is large compared with the vertical scale associated with wave components (under the restriction that the mean steepness ε remains small), and consequently is consistent for both narrowband and wideband wave fields. To achieve this, we describe the governing equations and the transformation (section 2) and use a perturbation expansion to find ordered solutions (section 3). We compare our solutions for monochromatic and bichromatic waves with numerical simulations and consider the significance for the prediction of near-surface wave kinematics of irregular random waves (section 4). Finally, we discuss the relation with conventional second-order theory, the wave-averaged near-surface flow (e.g., Stokes drift), and summarize our main conclusions (sections 5 and 6).

2. Governing equations in boundary-fitted coordinates

We consider surface gravity wave motion in an inviscid, incompressible fluid of constant density. The wave-induced

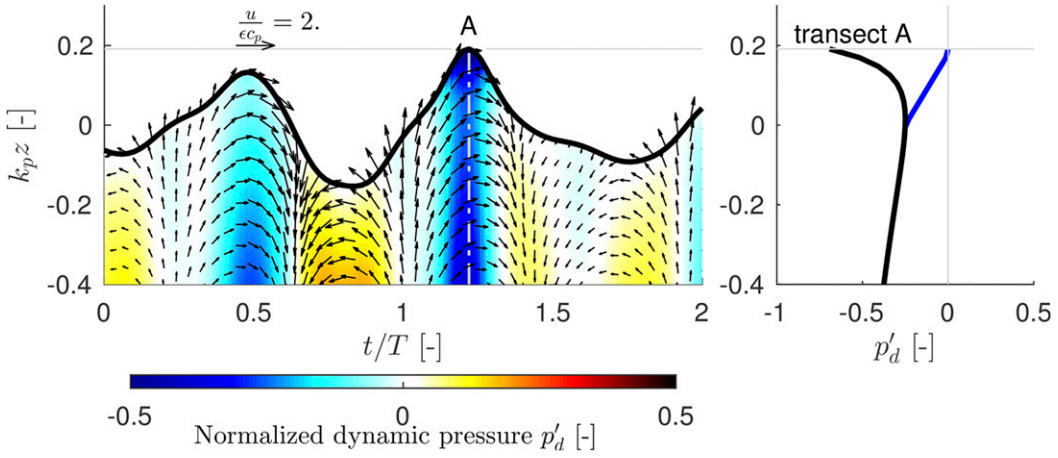

FIG. 1. Normalized dynamic pressure $p'_d = p_d/(\rho g H_{m_0})$ (with H_{m_0} the significant wave height) for a realization of a multidirectional irregular wave field based on a Jonswap spectrum (for details, see section 4c). Shown are (left) predicted pressure and superimposed velocity vectors predicted using the analytical extrapolation as a function of relative depth and time and (right) a comparison between analytical (black) and linear (blue) extrapolation of the dynamic pressure as a function of relative depth along transect A (white dashed–dotted line in left panel).

flow field is described in a Cartesian coordinate system where $\mathbf{x}^* = [x_1^*, x_2^*]$ and z^* are the horizontal and vertical coordinates, respectively. The fluid is vertically bounded between the bed at $z = -h$ (assumed constant in space and time) and the free-surface $z = \eta(\mathbf{x}^*, t^*)$ (with t^* time), and $z = 0$ denotes the unperturbed free-surface location. We define that mean surface elevation is zero (i.e., $\overline{\eta} = 0$, where $\overline{(\ldots)}$ denotes a suitable averaging operator). The velocity potential $\phi(\mathbf{x}^*, z^*, t^*)$ and the free-surface elevation $\eta(\mathbf{x}^*, t^*)$ are related by the governing equations (e.g., Mei et al. 2005)

$$\begin{aligned} \nabla_{x^*}^2\phi + \partial_{z^*}^2\phi &= 0 && -h \le z^* \le \eta, \\ \partial_{t^*}\phi + g\eta &= -\frac{1}{2}[|\nabla_{x^*}\phi|^2 + (\partial_{z^*}\phi)^2] && z^* = \eta, \\ \partial_{t^*}\eta - \partial_{z^*}\phi &= -\nabla_{x^*}\phi \cdot \nabla_{x^*}\eta && z^* = \eta, \\ \partial_{z^*}\phi &= 0 && z^* = -h, \end{aligned} \tag{2}$$

with $\nabla_x^* = [\partial_{x_1^*}, \partial_{x_2^*}]$. From top to bottom, these equations represent continuity (Laplace equation), the dynamic free-surface boundary condition, and the kinematic boundary conditions at the free surface and at the bed, respectively. The principal step in the present derivation is to replace the vertical coordinate z^* by a boundary-fitted coordinate, defined as

$$\mathbf{x} = \mathbf{x}^*, \quad t = t^*, \quad s = \frac{z^* - \eta(\mathbf{x}^*, t)}{D}, \quad D = h + \eta(\mathbf{x}^*, t). \tag{3}$$

In the new s-coordinate[1] system, the vertical domain transforms from $-h \le z^* \le \eta$ to $-1 \le s \le 0$. Further, although the horizontal coordinates $\mathbf{x}$ in the new coordinate system map one-to-one to the old coordinate systems, they denote the horizontal location along surfaces of constant s, and not constant height z. Hence, using this vertical transformation, the partial derivatives with respect to $\mathbf{x}^*$, t^*, and z^* transform as

$$\nabla_{x^*} = \nabla_x - \frac{(1+s)\nabla_x\eta}{D}\partial_s, \quad \partial_{t^*} = \partial_t - \frac{(1+s)\partial_t\eta}{D}\partial_s,$$
$$\partial_{z^*} = \frac{1}{D}\partial_s.$$

After substitution of these transformations into the potential equations, we obtain the transformed system[2]

$$\begin{aligned} \nabla_x^2\phi + \frac{\partial_s^2\phi}{h^2} &= \mathscr{S}, && -1 \le s \le 0, \\ \partial_t\phi + g\eta &= \mathscr{B}, && s = 0 \\ \partial_t\eta - \frac{\partial_s\phi}{h} &= \mathscr{K} && s = 0, \\ \partial_s\phi &= 0 && s = -1 \end{aligned} \tag{4}$$

[1] This coordinate system is widely referred to as the "σ-coordinate system." However, to avoid confusion with the use of σ as the (relative) angular frequency in the wave literature, we choose to use the alternative "s-coordinate" naming convention found in the literature.

[2] The transformed equations depend on D^{-m}, with $m = 1$ or 2. To separate linear from nonlinear terms, we multiplied the transformed equations with D^m and divided the results by h^m.

with

$$\mathscr{L} = \frac{(1+s)D}{h^2}(2\nabla_x\eta\cdot\nabla_x + \nabla_x^2\eta)\partial_s\phi - \frac{1+s}{h^2}|\nabla_x\eta|^2[2+(1+s)\partial_s]\partial_s\phi - \frac{2h\eta+\eta^2}{h^2}\nabla_x^2\phi,$$

$$\mathscr{B} = -\frac{1}{2h^2}[(\partial_s\phi)^2 + |D\nabla_x\phi - (1+s)\partial_s\phi\nabla_x\eta|^2] + \frac{(1+s)D}{h^2}\partial_t\eta\partial_s\phi - \frac{2h\eta+\eta^2}{h^2}(g\eta+\partial_t\phi),$$

$$\mathscr{K} = -\frac{D}{h}\nabla_x\eta\cdot\nabla_x\phi + \frac{1+s}{h}|\nabla_x\eta|^2\partial_s\phi - \frac{\eta\partial_t\eta}{h}. \tag{5}$$

Here the left-hand side corresponds to the usual terms of linear wave theory, whereas the terms on the right-hand side correspond to the nonlinear terms, which contain additional contributions due to the coordinate transformation. In particular, although the variable extent of the vertical domain (due to the moving free surface) is greatly simplified by the s-coordinate transformation, this simplification comes at the price of additional nonlinear terms in the potential equations. Most notable is the appearance of nonlinear forcing terms on the Laplace equation, which is a linear equation in Cartesian coordinates, due to the coordinate transformation.

The use of boundary-fitted coordinate systems is well established in large-scale ocean circulation models (e.g., Blumberg and Mellor 1987; Shchepetkin and McWilliams 2005). The transformation of the vertical coordinate to a boundary-fitted coordinate does not introduce any new approximation, and the transformed set [(4)] is entirely equivalent to the original nonlinear potential equations [(2)]. In fact, the transformed set can be used as a basis for nonlinear numerical codes that are applicable to nonbreaking strongly nonlinear waves (e.g., Engsig-Karup et al. 2009; Chalikov et al. 2014).

3. The ordered solution

To develop a series approximation for weakly nonlinear wave motion in deep to intermediate water depth, we define the nonlinearity parameter ε as the ratio between a characteristic amplitude and wavelength and assume that the waves are in intermediate [$kh = O(1)$] to deep water ($kh \gg 1$). To find ordered solutions, we introduce the usual perturbation expansions

$$\eta = \sum_{m=1}^{\infty}\eta^{(m)}, \quad \phi = \sum_{m=1}^{\infty}\phi^{(m)},$$

where $\eta^{(m)}$ and $\phi^{(m)}$ are assumed[3] to be of order ε^m. Since the lowest-order solution can be written as a superposition of free-plane waves,[4] we introduce the decomposition

$$\eta^{(1)}(\mathbf{x},t) = \sum_{\mathbf{k}_1,\mathscr{S}_1}\hat{\eta}_1^1 e_1^1, \quad \phi^{(1)}(\mathbf{x},z,t) = \sum_{\mathbf{k}_1,\mathscr{S}_1}\hat{\phi}_1^1 e_1^1.$$

Here $\mathbf{k}_1$ denotes the wavenumber, $\mathscr{S}_1 \in \{+,-\}$ is a sign index, $\hat{\eta}_1^1$ [and $\hat{\phi}_1^1(z)$] denotes the amplitude of the component with wavenumber $\mathbf{k}_1$ (subscript) and sign-index $\mathscr{S}_1$ (superscript). Furthermore,

$$e_n^n = \exp(i\mathbf{k}_n\cdot\mathbf{x} - i\omega_n t).$$

in which $\omega_n = \mathscr{S}_n\sigma_{\mathbf{k}_n}$ is the angular frequency that depends on $\mathbf{k}$ through the dispersion relation $\sigma_{\mathbf{k}}$ (with $\sigma > 0$). Further, since η and ϕ are real, we have

$$\hat{\eta}_1^{(m),+} = [\hat{\eta}_{-1}^{(m),-}]^* \quad \hat{\phi}_1^{(m),+} = [\hat{\phi}_{-1}^{(m),-}]^*,$$

where * denotes the complex conjugate and the subscript -1 refers to the component $-\mathbf{k}_1$. Further, anticipating that higher-order corrections consist of bound-wave components, the $O(\varepsilon^2)$ contributions are written as

$$\eta^{(2)}(\mathbf{x},t) = \sum_{\substack{\mathbf{k}_1,\mathbf{k}_2\\ \mathscr{S}_1,\mathscr{S}_2}}\hat{\eta}_{1,2}^{1,2}e_1^1e_2^2, \quad \phi^{(2)}(\mathbf{x},z,t) = \sum_{\substack{\mathbf{k}_1,\mathbf{k}_2\\ \mathscr{S}_1,\mathscr{S}_2}}\hat{\phi}_{1,2}^{1,2}(z)e_1^1e_2^2,$$

where $(\ldots)_{1,2}^{1,2} = (\ldots)_{\mathbf{k}_1,\mathbf{k}_2}^{\mathscr{S}_1,\mathscr{S}_2}$. Solutions for successive orders are found by substitution of the perturbation expansions into the governing set of equations [(4)] and collecting terms of like order.

a. The $O(\varepsilon)$ solution

At $O(\varepsilon)$ the Laplace equation is homogeneous and the boundary conditions are linear, so that after collecting terms up to $O(\varepsilon)$ and elimination of η from the kinematic and dynamic boundary conditions, we find the relations for $\hat{\phi}_1^1$ as

$$\left(\frac{1}{h^2}\partial_s^2 - k^2\right)\hat{\phi}_1^1 = 0 \quad -1\le s\le 0, \quad \text{and}$$

$$\left(-\omega_1^2 + \frac{g}{h}\partial_s\right)\hat{\phi}_1^1 = 0 \quad s = 0,$$

and $\partial_s\phi_1^1 = 0$ at $s = -1$. Hence, at this order, the problem is mathematically very similar to linear wave theory, and

[3] The ordering can be formalized using the scaling described in appendix B; for brevity and legibility, here we choose to solve the perturbed equations in dimensional variables.

[4] In the present work, we will neglect evanescent contributions to the wave field.

consequently, when parameterizing the result in terms of the free-surface amplitudes $\hat{\eta}_1^1$, the solution takes the familiar form

$$\hat{\phi}_1^1(s) = \Phi_1^1 \mathrm{Ch}_1^s, \quad \Phi_1^1 = \frac{-ig\hat{\eta}_1^1}{\omega_1}. \tag{6}$$

Here $\omega_1 = \mathscr{S}_1\sigma_1$ is related to $\mathbf{k}_1$ through the dispersion relation for linear waves $\sigma_1 = \sqrt{gk_1\tanh(k_1h)}$ and

$$\mathrm{Ch}_1^s = \frac{\cosh[k_1h(1+s)]}{\cosh(k_1h)} \quad -1 \le s \le 0.$$

The solution of (6) is different from the usual vertical solution of linear wave theory as it applies to the entire instantaneous water column. This becomes apparent when reverting back to Cartesian coordinates by substitution of $s = s(z, \eta)$, in which case we find $\hat{\phi}_1^1(z) = \Phi_1^1\mathrm{Ch}_1^z$ with

$$\mathrm{Ch}_1^z = \frac{\cosh\left\{\left[k_1\Big/\left(1+\frac{\eta}{h}\right)\right](h+z)\right\}}{\cosh(k_1h)} \quad -h \le z \le \eta.$$

Thus, when compared to the usual vertical structure of linear theory, the difference is the appearance of a factor $[1 + (\eta/h)]^{-1}$. In fact, at this order the solution for the velocity potential is equivalent to the stretched coordinate solution as proposed by Wheeler (1970) on heuristic grounds.

b. *The $O(\varepsilon^2)$ solution*

For the $O(\varepsilon^2)$ problem, we find that the second-order potential is governed by

$$(\partial_s^2 - k_{1,2}^2h^2)\phi_{1,2}^{1,2} = \mathscr{L}_{1,2}^{1,2} \quad -1 \le s \le 0, \quad \text{and} \tag{7a}$$

$$\left(-\omega_{1,2}^2 + \frac{g}{h}\partial_s\right)\phi_{1,2}^{1,2} = -i\omega_{12}\mathscr{B}_{1,2}^{1,2} - g\mathscr{K}_{1,2}^{1,2} \quad s = 0, \tag{7b}$$

with $\partial_s\hat{\phi}_{1,2}^{1,2} = 0$ at $s = -1$, $\omega_{1,2} = \omega_1 + \omega_2$, $\mathbf{k}_{1,2} = \mathbf{k}_1 + \mathbf{k}_2$, and where

$$\mathscr{L}_{1,2}^{1,2} = \frac{ig(1+s)}{2}\left[\frac{k_1k_{1,2}^2 - k_1^3}{\omega_1}\mathrm{Sh}_1(s) + \frac{k_2k_{1,2}^2 - k_2^3}{\omega_2}\mathrm{Sh}_2(s)\right] - \frac{ig}{h}\left[\frac{k_1^2}{\omega_1}\mathrm{Ch}_1(s) + \frac{k_2^2}{\omega_2}\mathrm{Ch}_2(s)\right],$$

$$\mathscr{K}_{1,2}^{1,2} = \frac{ih\omega_{1,2}}{2}\left[1 - \frac{g\mathbf{k}_1\cdot\mathbf{k}_2}{2\omega_1\omega_2}\right],$$

$$\mathscr{B}_{1,2}^{1,2} = -\left[\frac{\omega_1\omega_2}{2} + \frac{g^2\mathbf{k}_1\cdot\mathbf{k}_2}{2\omega_1\omega_2}\right].$$

Hence, at the second order, the solution procedure differs from that of conventional theory in that we have to solve an inhomogeneous boundary value problem. In general, the solution consists of the two homogeneous solutions and a particular solution. In this case, the particular solution that satisfies (7a)—as can be verified by substitution—is given by $\eta_1^1\eta_2^2\mathscr{P}_{1,2}^{1,2}(s)$ with

$$\mathscr{P}_{1,2}^{1,2}(s) = -\frac{ig(1+s)}{2}\left(\frac{k_1\mathrm{Sh}_1^s}{w_1} + \frac{k_2\mathrm{Sh}_2^s}{w_2}\right),$$

where

$$\mathrm{Sh}_1^s = \frac{\sinh[k_1h(1+s)]}{\cosh(k_1h)}.$$

The particular solution automatically satisfies the bottom boundary condition (i.e., $\partial_s\mathscr{P}_{1,2}^{1,2} = 0$ at $s = -1$), so that the homogeneous solution only consists of a contribution proportional to Ch_{1+2}, and the solution that solves (7a) and (7b) can be written as

$$\hat{\phi}_{1,2}^{1,2} = \left(\mathscr{K}_{1,2}^{1,2}\mathrm{Ch}_{1+2}^s + \mathscr{P}_{1,2}^{1,2}\right)\eta_1^1\eta_2^2, \tag{8}$$

with

$$\mathscr{K}_{1,2}^{1,2} = \frac{i\omega_{1,2}g^2}{\sigma_{1+2}^2 - w_{1,2}^2}\left[\frac{\mathbf{k}_1\cdot\mathbf{k}_2}{\omega_1\omega_2} - \frac{\omega_1\omega_2 + \omega_1^2 + \omega_2^2}{g^22} + \frac{(k_1^2\omega_2 + k_2^2\omega_1)}{2\omega_1\omega_2\omega_{12}}\right]. \tag{9}$$

The solution at this order thus consists of a term familiar from conventional second-order theory [the first term on the right of (8)] and a new term [the second-order term on the right of (8)], which has no comparable counterpart in conventional second-order theory and is the consequence of insisting that the complete second-order potential satisfies the Laplace equation in Cartesian coordinates (up to that order).

With the potential solution known, we obtain the expression for the second-order surface field using the dynamic boundary condition

$$\hat{\eta}_{1,2}^{1,2} = C_{1,2}^{1,2}\eta_1^1\eta_2^2, \tag{10}$$

with

$$C_{1,2}^{1,2} = \left(\frac{i\omega_{1,2}}{g}\mathscr{K}_{1,2}^{1,2} + \frac{\omega_1^2 + \omega_2^2 + \omega_1\omega_2}{2g} - g\frac{\mathbf{k}_1\cdot\mathbf{k}_2}{2\omega_1\omega_2}\right)$$

and $C_{1,2}^{1,2} = 0$ if $\mathbf{k}_1 + \mathbf{k}_2 = 0$ (because $\overline{\eta} = 0$ by definition), which is equivalent to the interaction coefficient from conventional theory relating the amplitude of the bound component to the forcing pair of primary waves (e.g., Hasselmann 1962; Herbers and Janssen 2016) Consequently, although the second-order potential is significantly modified near the crest because of the coordinate transformation, the solution for the second-order

surface elevation remains exactly the same as predicted by conventional theory.

c. Second-order near-crest velocity and pressure field

To find the horizontal velocities, we recall that the horizontal velocity is defined as the horizontal spatial gradient along planes of constant height (and not constant relative height),

$$\mathbf{u} = \nabla_{x^*}\phi = \nabla_x\phi + (\nabla_x s)\partial_s\phi, \quad w = \partial_{z^*}\phi = (\partial_z s)\partial_s\phi,$$

so that the velocities are given by

$$\mathbf{u} = \nabla_x\phi - \frac{1+s}{D}\nabla\eta\partial_s\phi = \nabla_x\phi - \frac{1+s}{h}\nabla\eta\partial_s\phi + O(\varepsilon^3), \quad \text{and}$$

$$w = \frac{1}{D}\frac{\partial\phi}{\partial s} = \frac{1}{h}\frac{\partial\phi}{\partial s} - \frac{\eta}{h^2}\frac{\partial\phi}{\partial s} + O(\varepsilon^3),$$

where we approximated $D^{-1} = (h+\eta)^{-1}$ using a Taylor series approximation. Although to the order of accuracy the Taylor approximation can be omitted, it simplifies the second-order expressions because of various cancellations while retaining the same accuracy. On substituting the second-order expressions for ϕ and η in these relations, and into the Bernouilli equation to obtain the pressure, retaining terms up to $O(\varepsilon^2)$, and returning back to Cartesian coordinates, we find

$$\begin{bmatrix}\mathbf{u}\\ w\\ p\end{bmatrix} = \begin{bmatrix}0\\ 0\\ p^{(0)}\end{bmatrix} + \sum_{\mathbf{k}_1,\mathscr{S}_1}\hat{\eta}_1^1\begin{bmatrix}\mathbf{U}_1^1\\ W_1^1\\ P_1^1\end{bmatrix}e_1^1 + \sum_{\substack{\mathbf{k}_1,\mathbf{k}_2\\ \mathscr{S}_1,\mathscr{S}_2}}\hat{\eta}_1^1\hat{\eta}_2^2\begin{bmatrix}\mathbf{U}_{1,2}^{1,2}\\ W_{1,2}^{1,2}\\ P_{1,2}^{1,2}\end{bmatrix}e_1^1e_2^2. \tag{11}$$

Here the $O(\varepsilon^0)$ contribution to the pressure is given by the hydrostatic contribution

$$p^{(0)} = \frac{\rho g(\eta - z)}{1 + (\eta/h)}.$$

For the first-order contributions, we find

$$\mathbf{U}_1^1 = \frac{g\mathbf{k}_1}{\omega_1}\mathrm{Ch}_1^z, \quad W_1^1 = -i\frac{gk_1^1}{\omega_1}\mathrm{Sh}_1^z,$$
$$P_1^1 = \rho g\left(\mathrm{Ch}_1^z - \frac{h+z}{h+\eta}\right), \tag{12}$$

where

$$\mathrm{Sh}_1^z = \frac{\sinh\left[\dfrac{k_1}{1+\dfrac{\eta}{h}}(h+z)\right]}{\cosh(k_1h)}.$$

The second-order contributions to the horizontal and vertical velocity and pressure can be written as

$$\mathbf{U}_{1,2}^{1,2} = i\mathbf{k}_{12}\mathscr{H}_{1,2}^{1,2}\mathrm{Ch}_{1+2}^z + \frac{g(h+z)}{2(h+\eta)}\left(\frac{\mathbf{k}_1k_1\mathrm{Sh}_1^z}{w_1} + \frac{\mathbf{k}_2k_2\mathrm{Sh}_2^z}{w_2}\right)$$
$$W_{1,2}^{1,2} = k_{12}\mathscr{H}_{1,2}^{1,2}\mathrm{Sh}_{1+2}^z - i\frac{g(h+z)}{2(h+\eta)}\left(\frac{k_1^2\mathrm{Ch}_1^z}{w_1} + \frac{k_2^2\mathrm{Ch}_2^z}{w_2}\right),$$
$$P_{1,2}^{1,2} = \frac{g(h+z)}{2(h+\eta)}(k_1\mathrm{Sh}_1^z + k_2\mathrm{Sh}_2^z) - iw_{12}\mathscr{H}_{1,2}^{1,2}\mathrm{Ch}_{1+2}^z$$
$$+ \frac{g^2}{2w_1w_2}[\mathbf{k}_1\cdot\mathbf{k}_2\mathrm{Ch}_1^z\mathrm{Ch}_2^z - k_1k_2\mathrm{Sh}_1^z\mathrm{Sh}_2^z]$$
$$- \frac{g(h+z)C_{1,2}^{1,2}}{h+\eta}. \tag{13}$$

Consequently, the linear part of the solutions only differ from conventional theory in the vertical structure function, but otherwise are identical to those obtained with conventional theory [cf. (12) with (A2) in appendix A]. The nonlinear contributions, on the other hand, also contain, in addition to terms that only differ in the vertical structure function, contributions that have no counterpart in the conventional description [cf. (13) with (A3a) and (A3b) in appendix A], and which are due to the movement of the surface.

4. Results

a. Monochromatic waves

To illustrate the difference with conventional theory and to verify our results, we consider a typical Stokes-type wave in deep and intermediate water. In this case, since we consider narrowband waves, for which the relative extrapolation distance remains of the order of the steepness $O(\varepsilon)$, so that differences between conventional theory and the present *s*-coordinate solution remain small and bounded. To assess the accuracy of the results, we compare predictions of both theories with results from streamfunction wave theory. Streamfunction wave theory was first introduced by Dean (1965) as an accurate numerical approximation for strongly nonlinear unidirectional waves of constant form and is still often used as a benchmark solution [we will use a solution by Dalrymple (1974)].

For $\varepsilon < 0.1$, crest velocities are similar when predicted using either stream theory, conventional theory, or the *s*-coordinate solutions in either deep $kd = 1$ or intermediate water $kd = 5$, and $u/(\varepsilon c)$ is generally proportional to ε for all solutions, indicative that second-order theory applies (Fig. 2). For $\varepsilon > 0.1$, streamfunction theory shows that $u/(\varepsilon c) \propto \varepsilon^2$, indicative that second-order

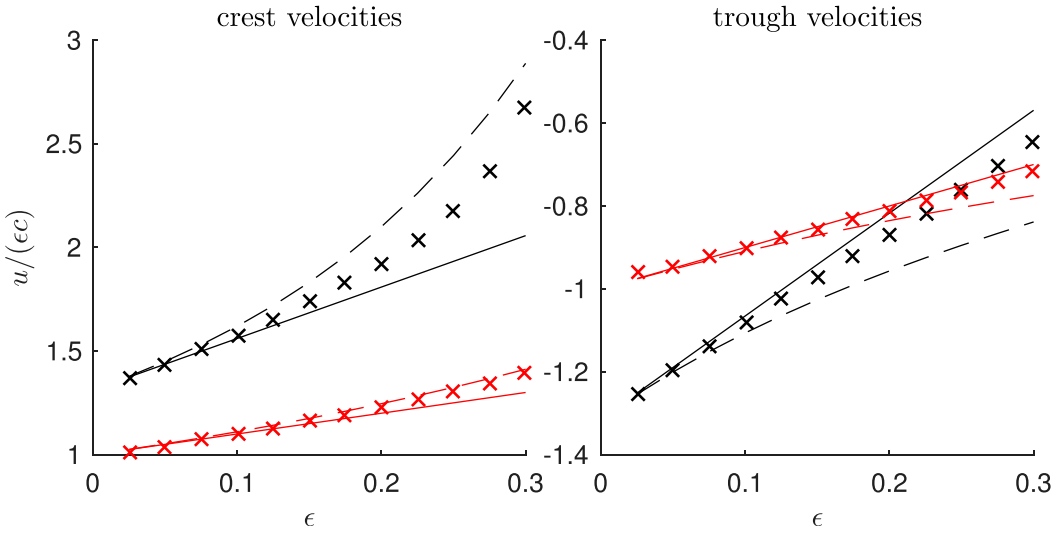

FIG. 2. Horizontal velocities at the (left) crest and (right) trough of a monochromatic wave as a function of the steepness ε in intermediate ($kh = 1$, red lines/markers) and deep ($kh = 5$, black lines/markers) water. Comparison between stream theory (markers), conventional theory (dashed lines), and the *s*-coordinate solution (solid lines).

theory is no longer strictly valid. As a consequence, both conventional and *s*-coordinate theory diverge from the streamfunction theory solution, and particularly so in intermediate water. Up to $\varepsilon = 0.2$ agreement with stream theory is reasonable for *s*-coordinate theory. In particular, near-trough velocities predicted by *s*-coordinate theory in intermediate water agree much better with streamfunction theory than the empirical methods.

Overall, when considering the near-surface velocity field under monochromatic waves, the *s*-coordinate theory provides slightly better results near the crests and troughs (Fig. 3). This mostly goes to show that the *s*-coordinate expressions are consistent, since in the limit of weakly nonlinear monochromatic (viz., narrowband) waves, the extrapolation methods are consistent to the order of approximation with the *s*-coordinate theory.

b. *Bichromatic waves*

Larger differences between the theories are expected when short components ride on the crests of longer components. To illustrate this and to verify the *s*-coordinate solutions, we consider the case of bichromatic unidirectional waves. Further, because stream theory does not apply for multicomponent waves, we compare results we consider simulation results computed with the Surface Waves till Shore (SWASH) nonhydrostatic time-domain model, which solves the Euler equations (Zijlema et al. 2011) as a reference solution. Because this is a time-domain model that requires an initial condition, we consider a standing wave solution in a closed 1D basin that can be initialized at $t = 0$ by prescribing the surface elevation alone (maximum elevation at the antinodes), while setting the velocity field to zero everywhere. This way we do not force the velocity field (either at the boundary or as an initial condition), but rather let it evolve naturally in the numerical model to minimize potential errors arising from the initialization.

For our simulations, we consider a basin with depth $h = 10$ m and length L. The wave field consists of two primary (or free) modes[5]: 1) a base component with frequency ω, amplitude a, and wavelength $2L$ of steepness $\varepsilon = 0.15$ in deep water ($kh = 5$) and 2) a shorter, secondary component with frequency $\omega_m = m\omega$ and amplitude a_m, with small steepness $\varepsilon_m = \varepsilon/5$ that has a wavenumber $k_m = m^2 k$.

At $t = 0$ both components are in phase and have a positive antinode at $x = 0$. For our comparisons, we are principally interested in the situation where the secondary component "rides" on the crest of the base component, occurring near $t = T_m/4$. At this moment the surface elevation of the base component is still near its maximum, but the velocity associated with the secondary component is nonzero. Because the range of the vertical motion is dominated by the low-frequency component [$a_m/a = O(m^{-2})$], we characterize the vertical scale with a. In this case we anticipate that the

[5] Arguably for each fundamental mode of the basin, the wave field is composed of a forward- and backward-propagating free wave; here we refer to this coupled pair as a single component/mode.

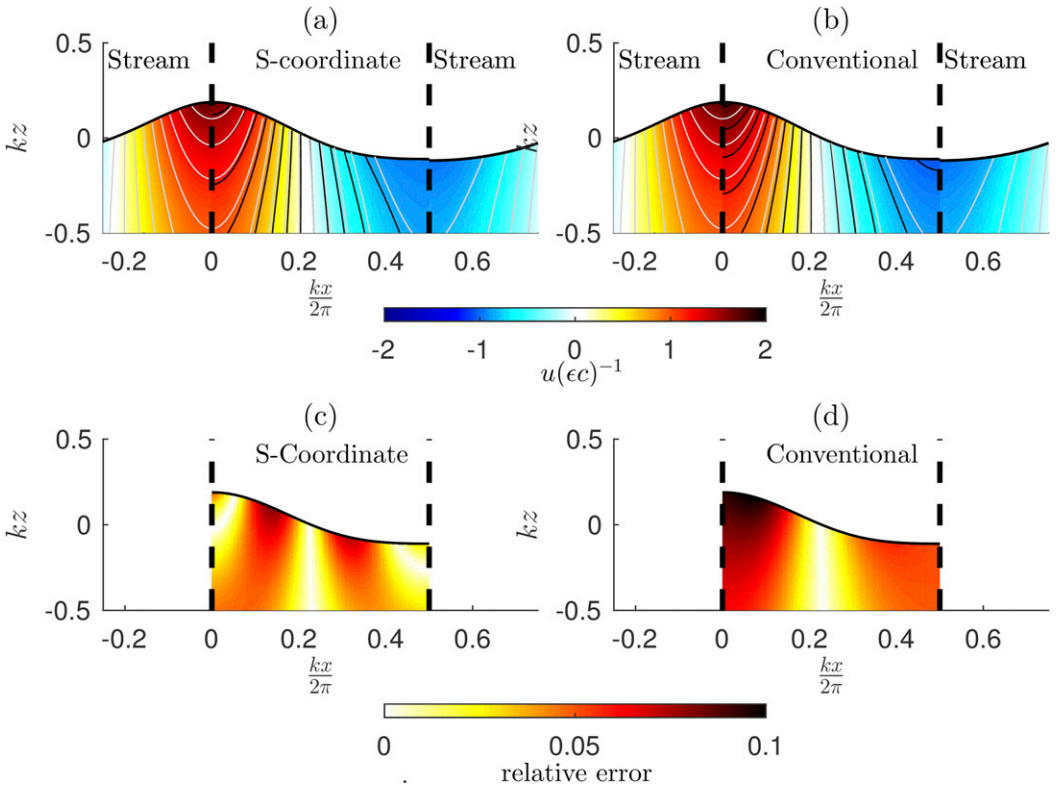

FIG. 3. Relative horizontal velocities $u/(\varepsilon c)$ (with $c = \omega/k$) below a monochromatic wave in intermediate water. Comparison between (a) stream theory solution (left and right of dashed lines) and the *s*-coordinate solution (between dashed lines); (b) as in (a), but now with conventional theory between dashed lines. Contours (thin lines) are drawn between −2 and 2 at an interval of 0.2, where the gray and black contours correspond to the stream theory solution and the black contours to the conventional/*s*-coordinate solutions, respectively. (c),(d) The relative errors between stream theory and conventional/*s*-coordinate solutions.

extrapolation of the short wave to the surface remains valid as long as $k_m a = O(m^2\varepsilon)$ does not approach $O(1)$.

To reproduce this case using SWASH, we discretize the basin vertically in 80 logarithmically distributed layers, where the layer thickness increases from top to bottom by 5% for each successive layer, thus ensuring a high resolution near the surface. Horizontally, we use a constant mesh size such that $\Delta x = L/640$, and the solution is marched in time from $t = 0$ until $t = T/8$ s (with T the wave period of the low-frequency component) using a time step of $\Delta t = T/1000$.

Evaluating the solution for secondary components with frequencies of 2–4 times the base component, we find that for $m = 2$ (with $k_m a = 0.6$) the three models predict very similar horizontal velocities near the free surface (Fig. 4). For $m = 3$ ($k_m a = 1$) small differences start to occur, as the conventional theory underpredicts velocities for $x/L \leq 0.075$ and generally shows small differences for $x/L \leq 0.15$. Overall, *s*-coordinate theory performs better, but up until this point the differences are not dramatic. However, for $m = 4$ (with $k_m a = 2$) conventional theory fails dramatically near the surface, whereas the *s*-coordinate solution retains good agreement with the SWASH results, both near the surface and further down in the water column (Fig. 5).

Surface velocities estimated from linear extrapolation are identical to *s*-coordinate theory, at the surface. Away from the surface, linear extrapolation results deviate from SWASH results, and they are identical to conventional theory for $z < 0$ (Fig. 5). In the far field from the surface, all three solutions converge and are identical, as would be expected.

In general, the *s*-coordinate solution accurately reproduces near-surface velocities, regardless of band separation of the bichromatic wave field. For wideband waves, the near-surface velocities predicted by conventional methods strongly diverge from the SWASH results and even away from the surface the velocity field can differ in these cases.

c. *Random sea state*

The principal motivation for the development of the present *s*-coordinate wave theory is to realistically

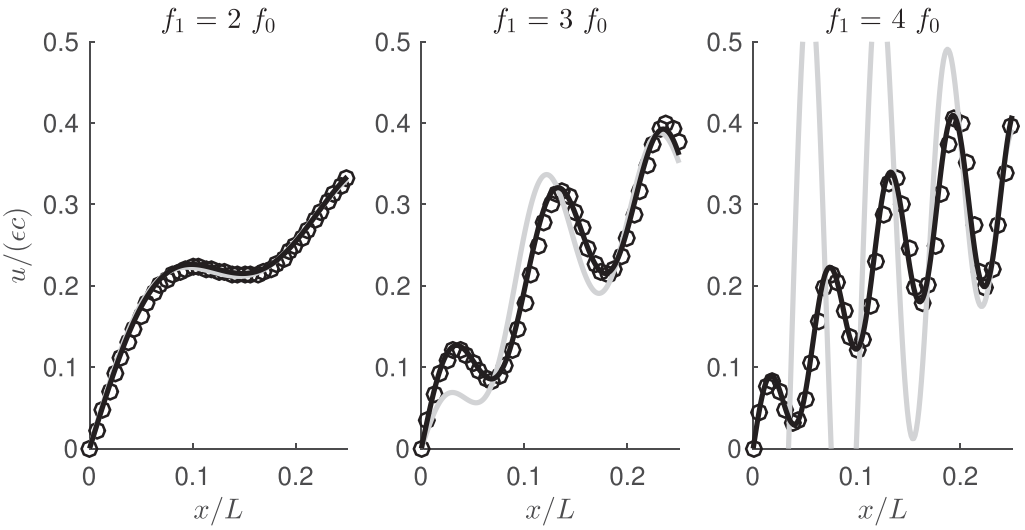

FIG. 4. Horizontal velocities along the surface for a bichromatic primary wave consisting of the fundamental basin mode and a higher free harmonic $\omega_m = m\omega$, evaluated for (from left to right) $m = 2, 3, 4$. The velocities are evaluated at $t = T_m/4$ along the first half of the basin. Comparison between velocities obtained using SWASH (markers), the s-coordinate solution (black line), and conventional theory (gray line).

reproduce near-surface kinematics in random seas. To illustrate the issues with conventional methods and the possible improvements by using the more consistent s-coordinate approach, we revisit the example considered in the introduction where we evaluate the pressure field below a steep unidirectional, random wave field ($\varepsilon = 0.15$). The wave field is generated using a directional spectrum $E(\omega, \theta) = 2E(\omega)\cos^2(\theta)/\pi$, where θ is the angular direction (radians) restricted to the half plane $-\pi/2 \le \theta \le \pi/2$. For the frequency distribution $E(\omega)$, we choose a Jonswap spectrum with $k_p d = 2$ (we set the water depth $d = 10\,\text{m}$ and k_p the peak wavenumber) and significant wave height $H_{m_0} = 4[\int E(\omega)\, d\omega]^{1/2}$. To construct a realization, we discretize the spectrum between $0.5\omega_p$ and $4\omega_p$ (with ω_p the peak angular frequency) and $-\pi/2 \le \theta \le \pi/2$ using 35 equidistant frequency meshes centered around frequencies $\omega_m = (1/2)\omega_p + m\Delta\omega$ and 30 equidistant directional meshes centered around $\theta_n = -\pi/2 + n\Delta\theta$. Each directional/frequency bin is associated with the primary wave (and its conjugate) with frequency ω_m, direction θ_n, amplitude $|\zeta_{m,n}| = (1/4)\sqrt{\Delta\omega\Delta\theta E(\omega_m, \theta_n)}$, and a phase $\arg(\zeta_{m,n})$ that is drawn from a random uniform distribution.

In contrast to the extrapolated results, the pressure field predicted with s-coordinate theory for the same (arbitrary) location and period of time as in Fig. 1 (using the same wave phases), consistently evaluates to zero along the surface (Fig. 6). Further, the pressure profile smoothly transitions from agreeing with conventional theory in the lower part of the water column to 0 at the surface, without the kink as observed when using linear extrapolation. A similar picture emerges when considering the horizontal and vertical velocity (Figs. 7a,b). Away from the surface the influence of high-frequency components attenuates, and the different approximations all predict similar values. Although linear extrapolation generally agrees with s-coordinate theory right at the surface, the horizontal velocity profile differs significantly in the near field of the surface. Further, the slope of the linearly extrapolated solution and the analytically extrapolated solution can differ dramatically at $z = 0$. The reason for this is that the slope is dominated by the nonlinear contributions, which are assumed constant above $z = 0$ for the linearly extrapolated profile (see appendix A). In other words, in the case of linear extrapolation, $\partial_z u$ at $z = 0$ is calculated based on the linear solution alone.

Differences between the solutions are much larger even if we consider components in excess of $4\omega_p$. For instance, when including components up to $5\omega_p$, the velocity profile changes dramatically, with only minimal changes in the surface elevation profile (Figs. 7c,d). This sensitivity illustrates that the extrapolation methods are not at all well behaved in the crest-to-trough region. In contrast, velocity profiles computed with s-coordinate theory remain physical, with changes in the profile due to presence of short waves confined to the near-surface regions, as would be expected.

5. Discussion

The s-coordinate wave theory introduced in the present work is based on a well-established vertical

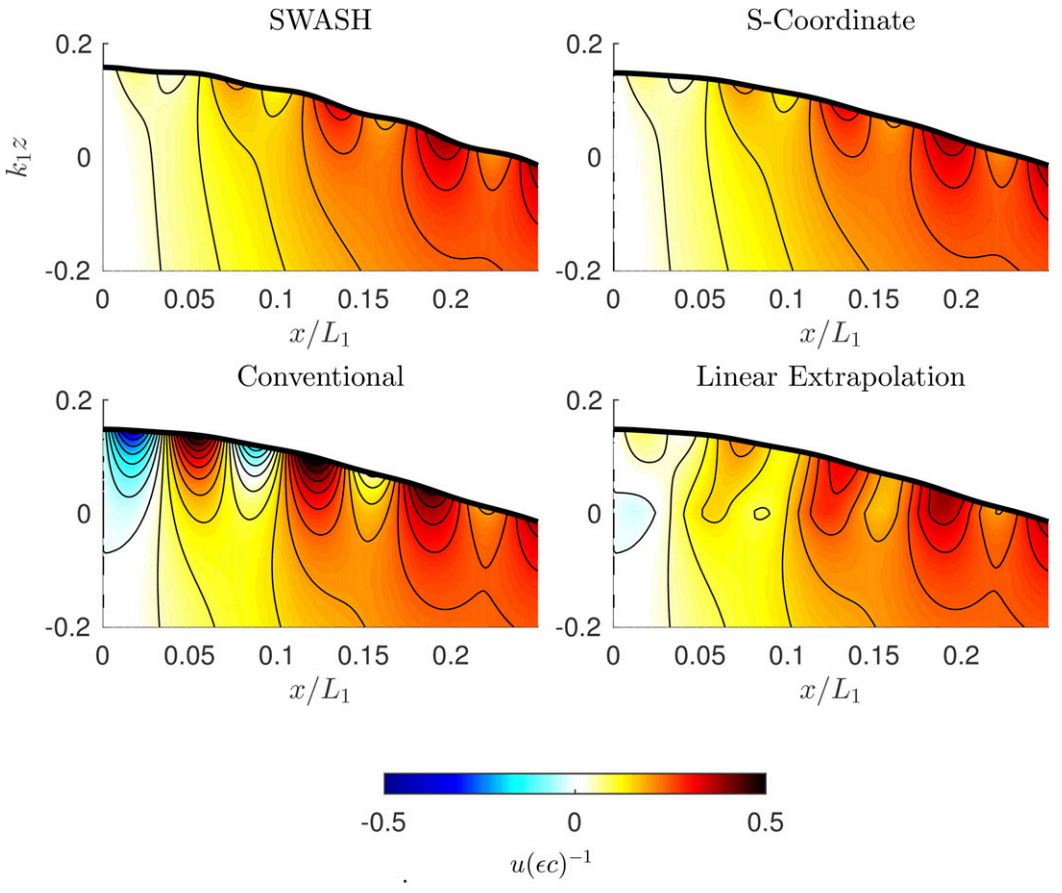

FIG. 5. Horizontal velocities below the bichromatic wave field in the first half of the basin evaluated at $t = T_m/4$ for the case where the short-wave component has a frequency of 4 times the base component.

coordinate transformation, which is suited to model fluid kinematics in the vicinity of a moving free surface. Our results are consistent with conventional second-order theory and include near-surface kinematics in wave fields of arbitrary bandwidth (which is not well-defined in conventional theory). The corrections in *s*-coordinate theory mostly affect the near-surface (and surface) kinematics, but do not significantly affect the second-order

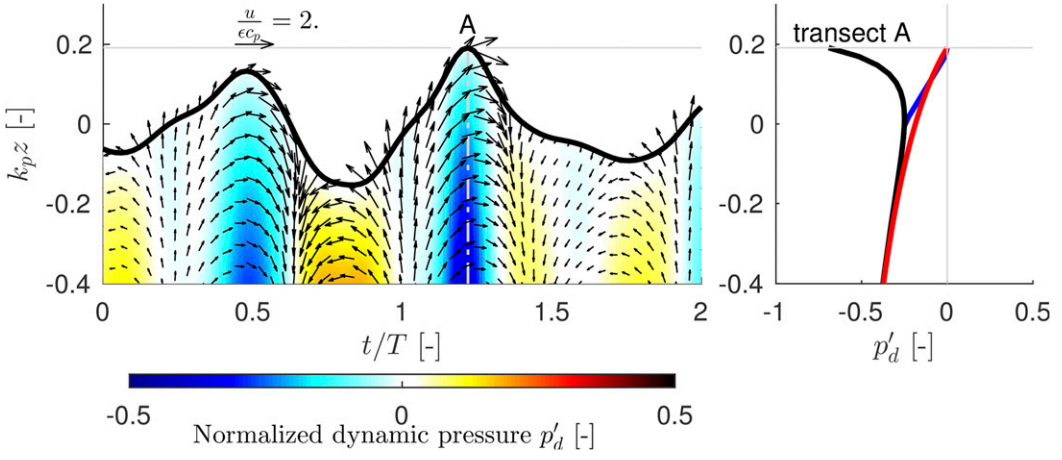

FIG. 6. Normalized dynamic pressure for the wave field as in Fig. 1, but the results shown in the left panel are computed using *s*-coordinate theory. The right panel shows a comparison between *s*-coordinate theory (red) and conventional theory using either an analytical (black) or linear (blue) extrapolation above $z > 0$.

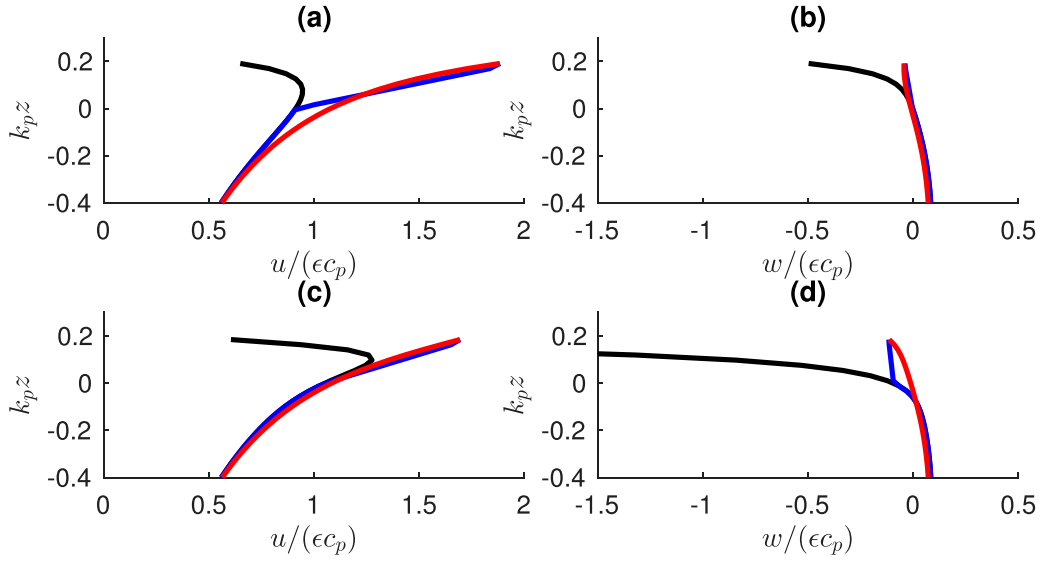

FIG. 7. Vertical profiles of the (a),(c) horizontal and (b),(d) vertical velocity under the crest at $t/T = 1.05$ (Fig. 6) predicted using s-coordinate (red), conventional (black), and linear extrapolation (blue above $z > 0$). Top panels are estimates of the velocity using a maximum frequency of $4f_p$ whereas the bottom panels include components up to $5f_p$.

free-surface elevation profile. We also see that linear extrapolation gives equivalent values for the wave kinematics as s-coordinate theory right at the surface (but not elsewhere) as long as the surface is positive. To investigate why this is the case, we consider the velocity potential at the surface as predicted by linear extrapolation

$$\phi(\eta) = \phi^{(1)}(0) + \phi^{(2)}(0) + [\eta^{(1)} + \eta^{(2)}]\frac{\partial \phi^{(1)}}{\partial z}\bigg|_{z=0}. \qquad (14)$$

The final term contributes up to $O(\varepsilon^3)$ and can thus be neglected, whereas the linearly extrapolated term has order $O(\varepsilon^2)$ and is thus part of the second-order solution. When we combine the two second-order terms and express them as a sum over the interacting pairs

$$\phi^{(2)}(0) + \eta^{(1)}\frac{\partial \phi^{(1)}}{\partial z}\bigg|_{z=0} = \sum_{\substack{\mathbf{k}_1,\mathbf{k}_2 \\ \omega_1,\omega_2}} \Phi^{1,2}_{1,2}\eta^1_1\eta^2_2, \qquad (15)$$

we find that the interaction coefficient is equivalent to the interaction coefficient from s-coordinate theory evaluated at the surface, that is, $\Phi^{1,2}_{1,2} = \phi^{1,2}_{1,2}(s = 0)$. Moreover, since the linear contributions at the surface are equal, the velocity potential predicted by s-coordinate theory is identical to that predicted by linear extrapolation [to $O(\varepsilon^2)$]. However, away from the surface the solutions are generally at variance (e.g., as illustrated in Fig. 7), with the s-coordinate producing the correct kinematics.

Also, away from the near-surface region, s-coordinate theory converges to conventional theory, as would be expected for the theory to be consistent with conventional second-order Stokes theory. To illustrate this, consider that in the region ($|z|/\varepsilon \gg 1$ for $z < 0$) components for which $k_1\eta_{\mathrm{rms}}$ is large, attenuate fast and can safely be neglected, whereas for longer components we have $k_1\eta = O(\varepsilon)$. Hence, the s-coordinate profile can be approximated by a first-order Taylor series in η around $\eta = 0$,

$$\mathrm{Ch}^z_1 \approx \widetilde{\mathrm{Ch}}^z_1 + k_1\eta\left(1 + \frac{z}{h}\right)\widetilde{\mathrm{Sh}}^z_1 + O(\varepsilon^2),$$

and similarly for Sh^z_1. When substituted in the expression for the velocity potential, the linear contribution reduces to the linear contribution of conventional Stokes theory. Furthermore, if we collect all second-order terms and express the result as a sum over interacting pairs, we find that the interaction coefficient also reduces to the interaction coefficient of conventional second-order theory (not shown).

The s-coordinate theory thus smoothly bridges the gap between the surface and a consistent solution to the field equations in the interior of the fluid ($z < 0$). Where conventional theory provides a solution to the Laplace equation for $z < 0$ while incorporating the surface boundary conditions up to $O(\varepsilon^2)$, the s-coordinate theory extends this to include the region $0 < z < \eta$. This is generally more consistent, but particularly important in random sea states characterized by large separation of length scales of the wave components (wideband).

The *s*-coordinate theory provides an approximate solution for the Laplace equation because we neglect terms of $O(\varepsilon^3)$ when solving the equations transformed to *s* coordinates. Historically, this has been a point of criticism of the linear (Wheeler) solution (Lo and Dean 1986), where imbalances occur at $O(\varepsilon^2)$. However, if Wheeler stretching is viewed as a first-order approximation, neglecting terms that are $O(\varepsilon^2)$—even if they occur in the Laplace equation—is entirely consistent with overall order of approximation.

The empirical methods have often been used to predict the velocity profile under strongly nonlinear waves, far outside the region where second-order theory applies. For such highly nonlinear wave profiles, well outside the validity range of second-order theory, there is of course no guarantee that the more consistent *s*-coordinate theory would perform well or better than empirical profiles specifically derived for that purpose. However, the *s*-coordinate theory presented here is a consistent second-order approximation, and for that reason should be preferred over more empirical methods to estimate the near-surface wave kinematics to that order of approximation.

Mean velocities and mass flux

Although the material transport due to the presence of ocean waves (or Stokes drift) is still not a fully resolved topic (e.g., Monismith et al. 2007), its existence is a well-known prediction of (weakly nonlinear) potential wave theory. Away from the surface, below trough level, theory predicts that the wave motion does not contribute to the mean Eulerian transport, but induces a mean Lagrangian mass transport. The *s*-coordinate wave theory as presented here is essentially a hybrid description that is horizontally Eulerian and vertically Lagrangian, which affects the interpretation of its mean properties. Further, it is known that the linear version of the theory (which is identical to Wheeler stretching) does not reproduce the proper (depth integrated) mass transport (Donelan et al. 1992) and in fact erroneously predicts a mean Eulerian flow below trough level. For these reasons it is important to verify that the mean properties of the second-order theory are consistent with known results.

Foremost, because the *s*-coordinate solutions converge to conventional results away from the crest–trough region (as discussed above), Eulerian averages in that region of the flow also vanish in that region (to the order considered). However, near the surface, Eulerian averages are not meaningful, as points above the lowest trough level are often outside the fluid domain. In contrast, the mean velocity along levels of constant *s* are always well defined and easy to compute in *s*-coordinate theory. However, this average along levels of constant *s* represents a quasi-Lagrangian average. To facilitate interpretation, we can assign a mean vertical position $\overline{z}$ in Cartesian space to averages in *s* by using the mean of the inverse transformation from $s \rightarrow z$, that is

$$\overline{z} = \overline{(h+\eta)s + \eta} = hs, \tag{16}$$

where $\overline{z}$ now represents the average location of a surface of constant *s*. In this case, the mean velocities along a level of constant *s* can be expressed in terms of $\overline{z}$ as

$$\overline{u}(\overline{z}) = \sum_{\mathbf{k}_1} \frac{g(h+\overline{z})k_1\mathbf{k}_1}{\omega_1 h} \mathrm{Sh}_1^{\overline{z}} E_{\mathbf{k}}. \tag{17}$$

Here, $E_{\mathbf{k}} = 2\zeta_{\mathbf{k}}\zeta_{\mathbf{k}}^*$ is the mean energy associated with component $\mathbf{k}$. At the mean location of the free surface $\overline{z} = 0$, this has the clear physical interpretation as the mean velocity measured along the free surface and reduces to $\omega\mathbf{k}E_{\mathbf{k}}$, or exactly half of the deep-water value of Stokes drift at the surface (e.g., Santala and Terray 1992).

Away from the free surface, a level of constant *s* no longer conforms to a material surface, and the mean $\overline{u}(\overline{z})$ no longer holds a clear physical significance. For instance, $\int_{-h}^{0} \overline{u}(\overline{z})\, d\overline{z}$ does not represent the wave-induced mass transport, because it does not account for the variation of the domain, and consequently, $\overline{u}(\overline{z})$ cannot be interpreted as a mean transport velocity (or mass flux). Instead, the wave-induced mass flux $\mathbf{Q}$ is found from integration over *s* of the mean value of the product of $\mathbf{u}$ and the Jacobian of the transformation $|\partial_s z| = h + \eta$,

$$\mathbf{Q} = \int_{-1}^{0} \overline{(h+\eta)u}\, ds = \sum_{\mathbf{k}} \frac{g\mathbf{k}E_{\mathbf{k}}}{\omega}, \tag{18}$$

and this does correspond to the usual definition of the wave-induced mass transport. In fact, all second-order depth-integrated mean wave properties (mean wave energy, energy flux, radiation stress) can be readily recovered in this way from the second-order solutions (appendix C, section a).

Consequently, *s* theory reproduces the integrated mass flux, and—using a proper transformation to a material-surface coordinate system—it reproduces the vertical distribution of mass transport otherwise known as the Stokes drift profile (appendix C, section b). However, a more natural way to define a vertically resolved mass-transport $\overline{\mathbf{u}}_m$ in the semi-Lagrangian framework is found by setting

$$\overline{\mathbf{u}}_m(\overline{z})d\overline{z} = \overline{(h+\eta)u}ds. \tag{19}$$

In this definition, $\overline{\mathbf{u}}_m(\overline{z})d\overline{z}$ describes the mean mass transport along *s* through a vertical plane $(h+\eta)ds$, and since $d\overline{z}$ does not change in time, the mean transport velocity is then found as

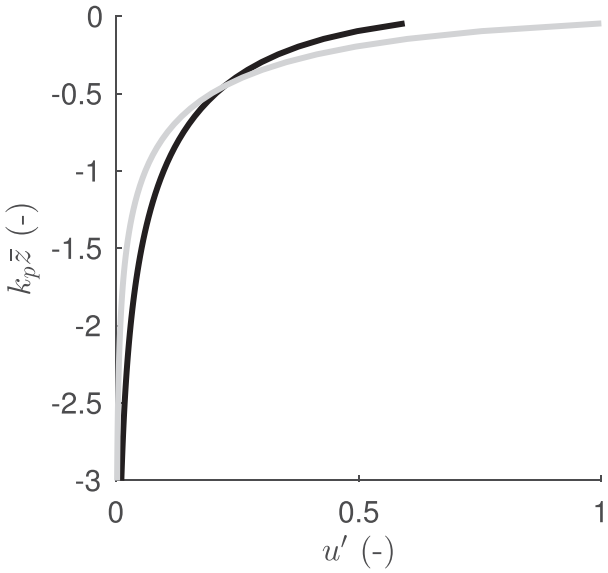

FIG. 8. Comparison between the normalized mean transport velocity u' obtained from (20) (black) and the Stokes drift profile [(C3), gray] in deep water for otherwise the same wave field as considered in section 4c. Both velocities are normalized with the Stokes drift velocity at $\overline{z} = 0$.

$$\overline{\mathbf{u}}_m(\overline{z}) = \sum_{\mathbf{k}_1} \frac{g\mathbf{k}_1 k_1}{\omega_1} \left(\frac{h+\overline{z}}{h} \mathrm{Sh}_1^{\overline{z}} + \frac{\mathrm{Ch}_1^{\overline{z}}}{k_1 h} \right) E_{\mathbf{k}_1}. \qquad (20)$$

This is a consistent definition of the mean mass flux within the context of our coordinate mapping. However, because levels of constant s do not correspond to material surfaces, it does not equal the usual Stokes drift. Compared with Stokes drift, mass transport defined this way is generally lower near $\overline{z} = 0$ but larger in the lower part of the water column (Fig. 8). However, both definitions result in the same vertically integrated mass flux $\mathbf{Q}$.

Clearly, Stokes drift is easier to physically interpret as it corresponds to the mean Lagrangian drift of a water particle. However, this makes it very difficult to observe directly as it requires a fully Lagrangian framework of observation. As a consequence, only indirect observational methods have been used in the field to estimate this Lagrangian transport (e.g., Lentz et al. 2008). The hybrid (Lagrangian in the vertical, Eulerian in the horizontal) transport equation (20) is possibly not so easily interpreted, but may be more amendable to observations. For instance, from a collocated observation of the free-surface and horizontal velocities, $\overline{\mathbf{u}}_m(\overline{z})$ can be estimated as

$$\overline{\mathbf{u}}_m(\overline{z}) = \overline{\left[1 + \frac{\eta(t)}{h}\right] \mathbf{u}\left\{\left[1 + \frac{\eta(t)}{h}\right]\overline{z} + \eta, t\right\}}.$$

Whether this is possible in the field or laboratory with current sensor technology remains to be seen, since it requires fairly high spatial and temporal sampling resolution in the near-surface region, which may be difficult to achieve due to attendant noise levels.

6. Conclusions

In this work we derived a second-order accurate description of the wave kinematics valid in the crest-to-trough region from first principles. Our results show that the profile first introduced by Wheeler (1970) on empirical grounds is essentially a consistent approximation, but it must be considered as a lowest order—or linear—estimate. For weakly nonlinear waves, additional higher-order corrections are required to obtain the correct (near) surface kinematics and to ensure that the mean properties—that is, the vanishing mean Eulerian flow and the Lagrangian mass flux (or Stokes drift)—are predicted correctly.

Near the surface, the s-coordinate solution is generally more consistent and robust than conventional second-order theory. However, the improvements in estimates of near-surface kinematics are particularly important and significant in natural random waves. For arbitrary sea states, the results from s-coordinate theory remain well behaved and consistent to the order of approximation without the need to introduce arbitrary cutoff frequencies or heuristically motivated approximations.

Acknowledgments. This research is supported by the U.S. Office of Naval Research (Littoral Geosciences and Optics Program and Physical Oceanography Program, Grant N000141612856), the National Oceanographic Partnership Program (Grant N000141310055), and the National Science Foundation (Physical Oceanography Program, Grant 1434864).

APPENDIX A

Conventional Second-Order Theory

Following the definitions as laid out in section 3, the second-order expressions for the velocity and pressure can be expressed as

$$\begin{bmatrix} \mathbf{u} \\ w \\ p \end{bmatrix} = \begin{bmatrix} 0 \\ 0 \\ p^{(0)} \end{bmatrix} + \sum_{\mathbf{k}_1, \mathscr{S}_1} \hat{\eta}_1^1 \begin{bmatrix} \tilde{\mathbf{U}}_1^1 \\ \tilde{W}_1^1 \\ \tilde{P}_1^1 \end{bmatrix} e_1^1 + \sum_{\substack{\mathbf{k}_1, \mathbf{k}_2 \\ \mathscr{S}_1, \mathscr{S}_2}} \hat{\eta}_1^1 \hat{\eta}_2^2 \begin{bmatrix} \tilde{\mathbf{U}}_{1,2}^{1,2} \\ \tilde{W}_{1,2}^{1,2} \\ \tilde{P}_{1,2}^{1,2} \end{bmatrix} e_1^1 e_2^2, \qquad (A1)$$

in which $p^{(0)} = -\rho g z$ and where for the first-order contributions we find

$$\tilde{\mathbf{U}}_1^1 = \frac{g\mathbf{k}_1}{\omega_1}\widetilde{\mathrm{Ch}}_1^z, \quad \tilde{W}_1^1 = -\mathrm{i}\frac{gk_1^1}{\omega_1}\widetilde{\mathrm{Sh}}_1^z, \quad \tilde{P}_1^1 = \rho g\widetilde{\mathrm{Ch}}_1^z, \tag{A2}$$

Further, the interaction coefficients relating pairs of surface amplitudes to second-order contributions are given by

$$\tilde{\mathbf{U}}_{1,2}^{1,2} = i\mathbf{k}_{12}\mathscr{H}_{1,2}^{1,2}\widetilde{\mathrm{Ch}}_{1+2}^z \quad \tilde{W}_{1,2}^{1,2} = k_{12}\mathscr{H}_{1,2}^{1,2}\widetilde{\mathrm{Sh}}_{1+2}^z \tag{A3a}$$

and

$$\tilde{P}_{1,2}^{1,2} = i(\omega_{1,2})\mathscr{H}_{1,2}^{1,2}\widetilde{\mathrm{Ch}}_{1+2}^z\frac{g^2\mathbf{k}_1\cdot\mathbf{k}_2\widetilde{\mathrm{Ch}}_1^z\widetilde{\mathrm{Ch}}_2^z - g^2k_1k_2\widetilde{\mathrm{Sh}}_1^z\widetilde{\mathrm{Sh}}_2^z}{\omega_1\omega_2} \tag{A3b}$$

with $\mathscr{H}$ defined as in the main text.

The vertical structure functions are defined for $-h \le z \le 0$ as

$$\widetilde{\mathrm{Ch}}_1 = \frac{\cosh[k_1(z+h)]}{\cosh(kh)}\widetilde{\mathrm{Sh}}_1 = \frac{\sinh[k_1(z+h)]}{\cosh(kh)}.$$

To evaluate the velocities and pressure for $z > 0$, we either simply continue the vertical profiles (analytical extrapolation) or when using linear extrapolation replace $\widetilde{\mathrm{Ch}}_1^z$ (and similarly $\widetilde{\mathrm{Sh}}_1^z$) with a Taylor series around $z = 0$, that is

$$\widetilde{\mathrm{Ch}}_1^z = 1 + k_1 z\tanh(k_1h) \quad 0 < z \le \eta^{(1)}, \quad \text{and}$$
$$\widetilde{\mathrm{Sh}}_1^z = \tanh(k_1h) + k_1 z \quad 0 < z \le \eta^{(1)}.$$

To be consistent with the boundary conditions evaluated to $O(\varepsilon^2)$, we truncate the Taylor series at the first order when evaluating the linear contributions [i.e., the linear term is assumed to be $O(\varepsilon^2)$]. Further, if z is above the first-order solution $\eta^{(1)}$, the solutions remain constant. For the second-order contributions, we neglect the linear term [which is $O(\varepsilon^3)$] and effectively assume that the second-order contributions are constant and equal to the contribution at $z = 0$ for $z > 0$.

APPENDIX B

Scaled Equations

Our objective is to seek approximate solutions for weakly nonlinear wave motion in deep to intermediate water and characterize the nonlinearity by the ratio ε between a characteristic amplitude a' and a characteristic vertical length scale L_v', such that $\varepsilon = a'/L_v'$. Here we and choose a generally applicable scaling and set $L_v = \hat{\mu}/k'$, where k' is a characteristic wavenumber and $\hat{\mu} = \tanh\mu$ is a revised dispersion parameter such that in the long-wave limit $\mu = k'h \ll 1$, we have $\hat{\mu} = \mu$, whereas in deep water $\hat{\mu} = 1$ (Beji 1995; Kirby 1998). We introduce the scaled variables

$$\tilde{\mathbf{x}}^* = k'\mathbf{x}^*, \quad \tilde{z}^* = k'z^*/\hat{\mu}, \quad \tilde{t}^* = k'c't^*,$$
$$\tilde{\eta} = \eta/a', \quad \tilde{\phi} = \frac{c'a'}{L_v'k'}\phi.$$

Here $\tilde{\mathbf{x}}^*$ is the scaled quantity corresponding to $\mathbf{x}^*$ (and similarly for $\tilde{z}$, $\tilde{\eta}$, etc.) and $c' = \sqrt{gL_v'}$ is a characteristic celerity (with g the gravitational acceleration). Subsequently, we introduce a boundary-fitted coordinate transformation defined as

$$\tilde{\mathbf{x}} = \tilde{\mathbf{x}}^*, \quad \tilde{t} = \tilde{t}^*, \quad \tilde{s} = \frac{\tilde{z}^* - \varepsilon\tilde{\eta}}{\tilde{D}}, \quad \tilde{D} = 1 + \frac{\hat{\mu}\varepsilon}{\mu}\tilde{\eta}, \tag{B1}$$

so that in the new coordinate system the vertical domain transforms from $-\mu/\hat{\mu} \le z \le \varepsilon\eta$ to $-\mu/\hat{\mu} \le s \le 0$ and $\partial_{\tilde{s}}\tilde{\phi}$ is still an $O(1)$ term. Furthermore, $\tilde{D}$ effectively represents the total water depth with the order parameter $\hat{u}\varepsilon/\mu$ representing the relative significance of the surface elevation on the total water. Using this vertical transformation, the partial derivatives with respect to $\overline{x}^*$, $\tilde{t}^*$, and $\tilde{z}^*$ transform as

$$\nabla_{\tilde{x}_j^*} = \nabla_{\tilde{x}} - \varepsilon\frac{\tilde{S}(\nabla_{\tilde{x}^*}\eta)}{\tilde{D}}\partial_s, \quad \partial_{\tilde{t}^*} = \partial_t - \varepsilon\frac{\tilde{S}(\partial_{\tilde{t}^*}\eta)}{\tilde{D}}\partial_s, \quad \partial_{\tilde{z}^*} = \frac{1}{\tilde{D}}\partial_s$$

with

$$\tilde{S} = 1 + \frac{\hat{\mu}\tilde{s}}{\mu}$$

where, because $\tilde{s}$ ranges from $\mu/\hat{\mu}$ till 0, the variable $\tilde{S}$ should be considered as an $O(1)$ term. Substitution of these definitions, and after multiplication with $\tilde{D}^2$, the potential equations become

$$\nabla_{\tilde{x}}^2\tilde{\phi} + \frac{1}{\hat{\mu}^2}\partial_{\tilde{s}}^2\tilde{\phi} = \tilde{\mathscr{L}} \quad -\mu/\hat{\mu} \le \tilde{s} \le 0,$$
$$\partial_{\tilde{t}}\tilde{\eta} - \frac{1}{\hat{\mu}^2}\partial_{\tilde{s}}\tilde{\phi} = \tilde{\mathscr{K}} \quad \tilde{s} = 0,$$
$$\tilde{\eta} + \partial_{\tilde{t}}\tilde{\phi} = \tilde{\mathscr{B}} \quad \tilde{s} = 0, \quad \text{and}$$
$$\frac{\partial\tilde{\phi}}{\partial\tilde{s}} = 0 \qquad \tilde{s} = -\mu/\hat{\mu},$$

with

$$\tilde{\mathscr{L}} = \varepsilon\tilde{S}[2\nabla_{\tilde{x}}\tilde{\eta}\cdot\nabla_{\tilde{x}}(\partial_{\tilde{s}}\tilde{\phi}) + (\nabla_{\tilde{x}}^2\tilde{\eta})\partial_{\tilde{s}}\tilde{\phi}] - 2\frac{\hat{\mu}\varepsilon}{\mu}\tilde{\eta}\nabla_{\tilde{x}}^2\tilde{\phi} + \frac{\hat{\mu}\varepsilon^2}{\mu}\tilde{S}[2\tilde{\eta}\nabla_{\tilde{x}}\tilde{\eta}\cdot\nabla_{\tilde{x}}(\partial_{\tilde{s}}\tilde{\phi}) - 2|\nabla_{\tilde{x}}\tilde{\eta}|^2\partial_{\tilde{s}}\tilde{\phi} + \tilde{\eta}(\nabla_{\tilde{x}}^2\tilde{\eta})\partial_{\tilde{s}}\tilde{\phi}]$$
$$- \varepsilon^2\tilde{S}^2|\nabla_{\tilde{x}}\tilde{\eta}|^2\partial_{\tilde{s}}^2\tilde{\phi} - \frac{\hat{\mu}^2\varepsilon^2}{\mu^2}\tilde{\eta}^2\nabla_{\tilde{x}}^2\tilde{\phi}.$$

$$\tilde{\mathscr{K}} = -\varepsilon\nabla_{\tilde{x}}\tilde{\eta}\cdot\nabla_{\tilde{x}}\tilde{\phi} - \frac{\hat{\mu}\varepsilon}{\mu}\tilde{\eta}\partial_{\tilde{t}}\tilde{\eta} - \frac{\hat{\mu}\varepsilon^2}{\mu}\tilde{\eta}\nabla_{\tilde{x}}\tilde{\eta}\cdot\nabla_{\tilde{x}}\tilde{\phi} + \varepsilon^2\tilde{S}|\nabla_{\tilde{x}}\tilde{\eta}|^2\partial_{\tilde{s}}\tilde{\phi},$$

$$\tilde{\mathscr{B}} = -\frac{\varepsilon}{2}[(\partial_{\tilde{s}}\tilde{\phi})^2 + |\nabla_{\tilde{x}}\tilde{\phi}|^2 - 2\tilde{S}\partial_{\tilde{t}}\tilde{\eta}\partial_{\tilde{s}}\tilde{\phi}] - \frac{2\hat{\mu}\varepsilon}{\mu}(\tilde{\eta}^2 + \tilde{\eta}\partial_{\tilde{t}}\tilde{\phi}) - \frac{\hat{\mu}^2\varepsilon^2}{\mu^2}(\tilde{\eta}^3 + \tilde{\eta}^2\partial_{\tilde{t}}\tilde{\phi}) + \varepsilon^2\tilde{S}\nabla_{\tilde{x}}\tilde{\phi}\cdot\nabla_{\tilde{x}}\tilde{\eta}\partial_{\tilde{s}}\tilde{\phi}$$
$$+ \frac{\hat{\mu}\varepsilon^2}{\mu}\tilde{S}\tilde{\eta}(\partial_{\tilde{t}}\tilde{\eta})\partial_{\tilde{s}}\tilde{\phi} + \frac{\hat{\mu}\varepsilon^3}{\mu}\tilde{S}\eta\nabla_{\tilde{x}}\tilde{\phi}\cdot\nabla_{\tilde{x}}\tilde{\eta}\partial_{\tilde{s}}\tilde{\phi} - \frac{\varepsilon^3}{2}\tilde{S}^2(\partial_{\tilde{s}}\tilde{\phi})^2|\nabla_{\tilde{x}}\tilde{\zeta}|^2.$$

The transformation into the new coordinate system introduces a host of terms not present in the original Cartesian problem. In particular, the equations now give rise to higher-order nonlinear terms up to $O(\varepsilon^3)$ and terms that scale as $\hat{\mu}^n\varepsilon^m/\mu^n$. The later terms originate from the denominator of the transformation defined in (B1) and effectively express that when the water is deep, that is, $\mu \gg 1$ [such that $\hat{\mu} = O(1)$], the contribution of the surface elevation to the total depth can be neglected in the transformation (B1), and these additional terms can be safely ignored. However, in intermediate to shallow water, as $\hat{\mu}/\mu = O(1)$ these terms contribute at the orders ε^m and should be included to the order of the approximation in ε pursued.

Finally, we remark that for a Stokes-type perturbation to be tenable, as done in the main text, we have to restrict ourselves to a short-wave scaling, or in other words the dispersive parameter $\hat{\mu}$ has to be $O(1)$. In this case $\varepsilon = k'a$ represents the usual wave steepness. However, in light of the discussion above, the most interesting dynamics occur when $\mu/\hat{\mu} = O(1)$, and since $\tanh(1) = O(1)$ we tacitly assume water of intermediate depth, that is, $\mu = O(1)$ as well.

APPENDIX C

Mean Wave Properties

a. Depth-integrated properties

Important depth-integrated second-order mean dynamical quantities such as the mass flux $\mathbf{Q}$ (or pseudowave momentum), wave energy E, the energy flux $\mathbf{F}$, and the radiation stress $S_{1,2}$ are within the context of conventional wave theory all derivable from the first-order solutions. However, because in s-coordinate theory the mean second-order velocity does not vanish, the full second-order solutions are required when these properties are derived from the expressions formulated in s coordinates. Denoting the vertically resolved quantity corresponding related to the depth integrated property as $f(s)$, the mean-integrated quantities are given by

$$\rho\overline{\int_{-d}^{\eta} f(z)\,dz} = \rho\int_{-1}^{0} h\overline{f} + \overline{\eta f}\,ds$$

because $dz = (h+\eta)ds$. When we substitute the ordered solutions and retain terms up to $O(\varepsilon^2)$, take the spatial and temporal average, and perform the vertical integration, we obtain for the wave energy

$$E = \rho\int_{-1}^{0}\left(\frac{h}{2}\overline{|\mathbf{u}^{(1)}|^2} + \frac{h}{2}\overline{[w^{(1)}]^2} + g(1+s)\{h\overline{\eta^{(2)}} + \overline{[\eta^{(1)}]^2}\}\right)ds$$
$$= \sum_{\mathbf{k}} E_{\mathbf{k}}, \tag{C1}$$

where $E_{\mathbf{k}} = 2a_{\mathbf{k}}^{+}a_{-\mathbf{k}}^{-}$ is the mean energy associated with a component $\mathbf{k}$. Similarly, expressions the mass flux, energy flux, and radiation stress become

$$\mathbf{Q} = \int_{-1}^{0}[h\overline{\mathbf{u}^{(2)}} + \overline{\eta^{(1)}\mathbf{u}^{(1)}}]\,ds = \sum_{\mathbf{k}}\frac{\mathbf{k}}{k}\frac{E_{\mathbf{k}}}{c},$$
$$\mathbf{F} = h\int_{-1}^{0}\overline{p^{(1)}\mathbf{u}^{(1)}}\,ds = \sum_{\mathbf{k}}\frac{\mathbf{k}c_g}{k}E_{\mathbf{k}}, \quad \text{and}$$
$$S_{1,2} = \int_{-1}^{0}[h\overline{u_1^{(1)}u_2^{(1)}} + h\overline{p^{(2)}} + \overline{p^{(1)}\eta^{(1)}}]\,ds$$
$$= \left[\frac{k_1k_2}{k^2}\frac{c_g}{c} + \delta_{1,2}\left(\frac{c_g}{c} - \frac{1}{2}\right)\right]E_{\mathbf{k}},$$

where

$$c = \frac{\omega}{k}, \quad c_g = \left[\frac{1}{2} + \frac{kh}{\sinh(2kh)}\right]c, \tag{C2}$$

are the usual definitions of the wave celerity and group velocity, respectively. Consequently, to $O(\varepsilon^2)$, the present theory is in full agreement with established results.

b. Stokes drift

To show that the s-coordinate solutions are consistent with the usual definition of a mass transport velocity, we define a material coordinate system (similar to Mellor 2015)

$$z(\mathbf{x}, s', t) = s'h + \zeta(s', t),$$

where $z(\mathbf{x}, s', t)$ denotes the instantaneous location of a material surface that on average is located at $s'h$, and ζ is the instantaneous displacement of the material surface, which to $O(\varepsilon^2)$ is given by

$$\zeta(s', t) \approx \int_0^{t'} w(s, t')|_{s=s'}\, dt' = \sum_{\mathbf{k}_1, s_1} \hat{\zeta}_1^1 \frac{gk_1}{\omega_1^2} \mathrm{Sh}_1^s \Big|_{s=s'} e_1^1.$$

Expressing $\mathbf{u}(s)$ in terms of s' and following the same procedure as before but now averaging in time while keeping s' constant and noting that we have $\overline{z} = hs'$, we arrive at

$$\overline{\mathbf{u}}_m(\overline{z}) = \overline{\mathbf{u} \frac{dz}{ds'} \frac{ds'}{d\overline{z}}} = \sum_{\boldsymbol{k}} \frac{2g\mathbf{k}k}{\omega} \frac{\cosh[2k(h+\overline{z})]}{\sinh(2kh)} E_{\mathbf{k}}, \qquad \text{(C3)}$$

which corresponds to the usual definition of the mean mass transport velocity (or Stokes drift). Hence, the definition from (20) is consistent with (C3), and the differences are due to a different way of accounting for the vertical motion in the averaging process.

REFERENCES

Baldock, T. E., C. Swan, and P. H. Taylor, 1996: A laboratory study of nonlinear surface waves on water. *Proc. Trans. Roy. Soc. London*, **A354**, 649–676, doi:10.1098/rsta.1996.0022.

Beji, S., 1995: Note on a nonlinearity parameter of surface waves. *Coast. Eng.*, **25**, 81–85, doi:10.1016/0378-3839(94)00031-R.

Blumberg, A. F., and G. L. Mellor, 1987: A description of a three-dimensional coastal ocean circulation model. *Three-Dimensional Coastal Ocean Models*, N. S. Heaps, Ed., Coastal and Estuarine Sciences, Vol. 4, Amer. Geophys. Union, 1–16,

Chalikov, D., A. V. Babanin, and E. Sanina, 2014: Numerical modeling of 3D fully nonlinear potential periodic waves. *Ocean Dyn.*, **64**, 1469–1486, doi:10.1007/s10236-014-0755-0.

Dalrymple, R. A., 1974: A finite amplitude wave on a linear shear current. *J. Geophys. Res.*, **79**, 4498–4504, doi:10.1029/JC079i030p04498.

Dean, R. G., 1965: Stream function representation of nonlinear ocean waves. *J. Geophys. Res.*, **70**, 4561–4572, doi:10.1029/JZ070i018p04561.

Deng, Y., J. Yang, W. Zhao, X. Li, and L. Xiao, 2016: Freak wave forces on a vertical cylinder. *Coast. Eng.*, **114**, 9–18, doi:10.1016/j.coastaleng.2016.03.007.

Donelan, M. A., F. Anctil, and J. C. Doering, 1992: A simple method for calculating the velocity field beneath irregular waves. *Coast. Eng.*, **16**, 399–424, doi:10.1016/0378-3839(92)90061-X.

Engsig-Karup, A. P., H. B. Bingham, and O. Lindberg, 2009: An efficient flexible-order model for 3D nonlinear water waves. *J. Comput. Phys.*, **228**, 2100–2118, doi:10.1016/j.jcp.2008.11.028.

Geng, X., M. C. Boufadel, T. Ozgokmen, T. King, K. Lee, Y. Lu, and L. Zhao, 2016: Oil droplets transport due to irregular waves: Development of large-scale spreading coefficients. *Mar. Pollut. Bull.*, **104**, 279–289, doi:10.1016/j.marpolbul.2016.01.007.

Hasselmann, K., 1962: On the non-linear energy transfer in a gravity-wave spectrum, Part I. General theory. *J. Fluid Mech.*, **12**, 481–500, doi:10.1017/S0022112062000373.

Herbers, T. H. C., and T. T. Janssen, 2016: Lagrangian surface wave motion and stokes drift fluctuations. *J. Phys. Oceanogr.*, **46**, 1009–1021, doi:10.1175/JPO-D-15-0129.1.

——, P. F. Jessen, T. T. Janssen, D. B. Colbert, and J. H. MacMahan, 2012: Observing ocean surface waves with GPS-tracked buoys. *J. Atmos. Oceanic Technol.*, **29**, 944–959, doi:10.1175/JTECH-D-11-00128.1.

Kirby, J. T., 1998: Discussion of 'Note on a nonlinearity parameter of surface waves' by S. Beji. *Coast. Eng.*, **34**, 163–168, doi:10.1016/S0378-3839(98)00024-6.

Lentz, S. J., M. Fewings, P. Howd, J. Fredericks, and K. Hathaway, 2008: Observations and a model of undertow over the inner continental shelf. *J. Phys. Oceanogr.*, **38**, 2341–2357, doi:10.1175/2008JPO3986.1.

Lo, J. M., and R. G. Dean, 1986: Evaluation of a modified stretched linear wave theory. *Proc. 20th Conf. Coastal Engineering*, Taipei, Taiwan, ASCE, 522–536, doi:10.1061/9780872626003.040.

Longuet-Higgins, M. S., and R. W. Stewart 1960: Changes in the form of short gravity waves on long waves and tidal currents. *J. Fluid Mech.*, **8**, 565–583, doi:10.1017/S0022112060000803.

Mei, C. C., M. Stiassnie, and D. K.-P. Yue, 2005: *Theory and Applications of Ocean Surface Waves*. Advanced Series on Ocean Engineering, Vol. 23, World Scientific, 1136 pp.

Mellor, G., 2015: A combined derivation of the integrated and vertically resolved, coupled wave–current equations. *J. Phys. Oceanogr.*, **45**, 1453–1463, doi:10.1175/JPO-D-14-0112.1.

Monismith, S. G., E. A. Cowen, H. M. Nepf, J. Magnaudet, and L. Thais, 2007: Laboratory observations of mean flows under surface gravity waves. *J. Fluid Mech.*, **573**, 131–147, doi:10.1017/S0022112006003594.

Rascle, N., B. Chapron, A. Ponte, F. Ardhuin, and P. Klein, 2014: Surface roughness imaging of currents shows divergence and strain in the wind direction. *J. Phys. Oceanogr.*, **44**, 2153–2163, doi:10.1175/JPO-D-13-0278.1.

Rodenbusch, G., and G. Z. Forristall, 1986: An empirical model for random directional wave kinematics near the free surface. *Offshore Technology Conf.*, Houston, TX, Offshore Technology Conference, 10 pp., doi:10.4043/5097-MS.

Santala, M. J., and E. A. Terray, 1992: A technique for making unbiased estimates of current shear from a wave-follower. *Deep-Sea Res. I*, **39**, 607–622, doi:10.1016/0198-0149(92)90091-7.

Schløer, S., H. Bredmose, and H. B. Bingham, 2011: Irregular wave forces on monopile foundations: Effect of full nonlinearity and bed slope. *ASME 2011 30th Int. Conf. Ocean, Offshore and Arctic Engineering*, Rotterdam, Netherlands,

American Society of Mechanical Engineers, 581–588, doi:10.1115/OMAE2011-49709.

Sharma, J. N., and R. G. Dean, 1981: Second-order directional seas and associated wave forces. *Soc. Pet. Eng. J.*, **21**, 129–140, doi:10.2118/8584-PA.

Shchepetkin, A. F., and J. C. McWilliams, 2005: The Regional Oceanic Modeling System (ROMS): A split-explicit, free-surface, topography-following-coordinate oceanic model. *Ocean Modell.*, **9**, 347–404, doi:10.1016/j.ocemod.2004.08.002.

Stokes, G. G., 1847: On the theory of oscillatory waves. *Trans Cambridge Philos. Soc.*, **8**, 441–473.

Wheeler, J. D., 1970: Method for calculating forces produced by irregular waves. *J. Pet. Technol.*, **22**, 359–367, doi:10.2118/2712-PA.

Zijlema, M., G. S. Stelling, and P. B. Smit, 2011: SWASH: An operational public domain code for simulating wave fields and rapidly varied flows in coastal waters. *Coastal Eng.*, **58**, 992–1012, doi:10.1016/j.coastaleng.2011.05.015.